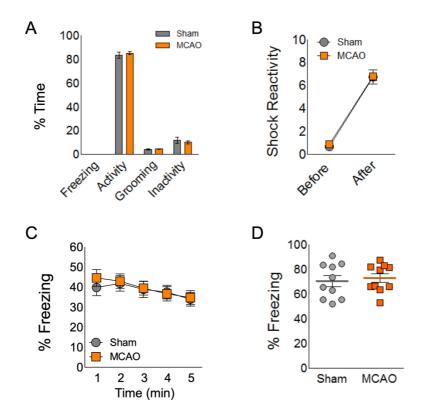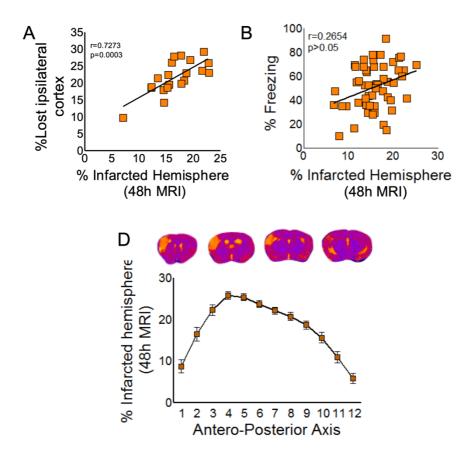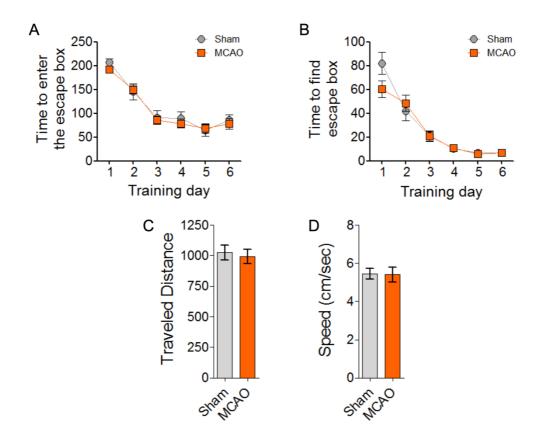**Supplementary figure 1. Cortical ischemia induces hippocampal-dependent cognitive impairment. (A)** Percentage of freezing in sham and MCAO mice during familiarization in contextual fear conditioning (CFC; 150s before receiving foot-shocks). Graph bars also display the % of time spent by both sham and MCAO in different behaviours such as activity, inactivity and grooming ($p>0.05$ vs. sham; sham, n=8; MCAO, n=9). **(B)** Quantification of foot-shock reactivity in sham and MCAO mice during CFC training as an indicator of nociception in CFC. Data represent the ratio between the travelled distance during the 5 seconds immediately after the foot-shock and the travelled distance during the 5 seconds just before the foot-shock. Data are displayed as arbitrary units (AU). Two-way ANOVA demonstrated a significant effect of shock in both sham and MCAO groups ($F_{(1,15)}= 279.15$; $p<0.05$ before vs. after; sham, n=8; MCAO, n=9). **(C)** Percentage of freezing response in sham and MCAO groups 1 hour after CFC. Two-way ANOVA demonstrated a significant effect on time ($F_{(4,32)}= 6.85$; $p<0.05$, 1 vs. 5min; sham, n=9; MCAO, n=9) but no differences were observed between sham and MCAO. **(D)** Memory retention 24h after MCAO calculated as percentage of freezing response (*$p<0.05$ vs. sham; sham, n=10; MCAO, n=10). Data are mean $\pm$ SEM. Data were compared by using nonparametric 2-tailed Mann-Whitney tests or a nonparametric 2-way ANOVA followed by Bonferroni post hoc testing.
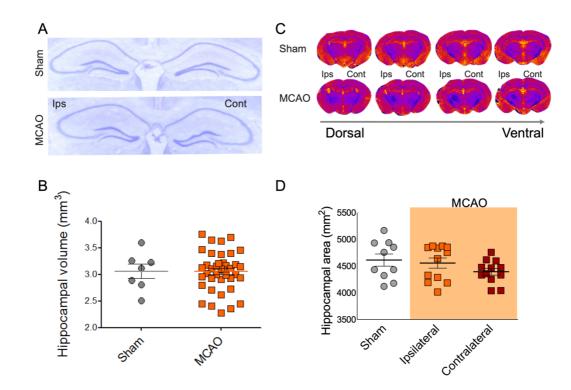
Supplementary figure 2. Cognitive impairment after MCAO does not correlate with lesion size and location. (A) Spearman correlation between initial infarct volume (MRI; 48h after surgery) and final lesion size determined by Nissl staining (35 days after) and calculated as percentage of ipsilesional cortex lost (Spearman r=0.7273, p=0.0003; MCAO, n=20). **(B)** Spearman correlation between freezing response and infarct volume determined 48h after cerebral ischemia by MRI. Linear regression analysis is also displayed in the graph (Spearman r=0.2654, p=0.0548; MCAO, n=53). **(C)** Percentage of infarcted hemisphere along the anterior-posterior axis determined 48h after MCAO by MRI (MCAO, n=34 animals)**.** Data are mean ± SEM. Data were compared by using nonparametric 2-tailed Spearman correlation.
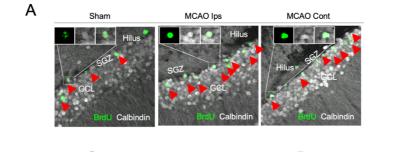
Supplementary figure 3. Cortical ischemia affects long-term spatial memory. (A-B) Time spent to enter (A) or to find (B) the escape box (in seconds) throughout the trials of the training phase of Barnes maze. Two-way ANOVA demonstrated a significant effect on time to enter ($F_{(5,170)}$= 62.79; $p<0.0001$, day 1 vs. day 6) or to find the escape box ($F_{(5,190)}$= 67.18; $p<0.0001$, day 1 vs. day 6; sham, n=12; MCAO, n=19) but no differences were observed between sham and MCAO. **(C)** Total distance (in cm) travelled by sham and ischemic mice during training phase in the Barnes maze platform (sham, n=12; MCAO, n=19). **(D)** Averaged speed (cm/s) showed by sham and ischemic mice during Barnes maze training (sham, n=12; MCAO, n=19). Data are mean ± SEM. Data were compared by using nonparametric 2-tailed Mann-Whitney tests or a nonparametric 2-way ANOVA followed by Bonferroni post hoc testing.
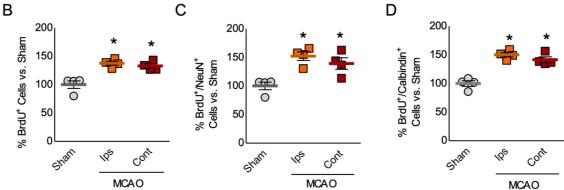
Supplementary figure 4. Total hippocampal volume and area are not affected by cortical ischemia. (A-B) Quantification of dorsal hippocampal volume in sham and MCAO mice determined by Nissl staining and Cavalieri estimation 1 month after surgery. Representative images of Nissl staining from each group are displayed in panel A (sham, n=7; MCAO, n=36). **(C-D)** Quantification of hippocampal area determined 2 months after surgery by ex-vivo MRI of sham and ischemic fixed brains. Representative MRI images are shown in C (Sham, n=10; MCAO ips, n=12; MCAO cont, n=12). Data are mean ± SEM. Data were compared by using nonparametric 2-tailed Mann-Whitney tests.
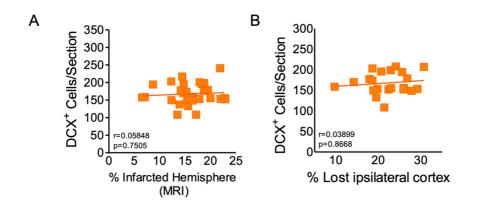
Supplementary figure 5. Ischemia increases hippocampal neurogenesis. (A-D)
Quantification of the number of newborn neurons 65 days after stroke. BrdU$^+$ cells (B) and newborn neurons BrdU$^+$/NeuN$^+$ (C) or BrdU$^+$/calbindin$^+$ (D) 65 days after surgery in sham and MCAO. BrdU (100mg/Kg) was administered during the second and third week after surgery coinciding with the proliferative peak for Ki67 determined in Figure 3E. Data are expressed as % of sham (*p<0.05 vs sham; n= 4 for both sham and MCAO groups). Representative images of newborn neurons are displayed in A. Scale bar: 20μm. Data are mean ± SEM. Data were compared by using nonparametric 2-tailed Mann-Whitney tests.
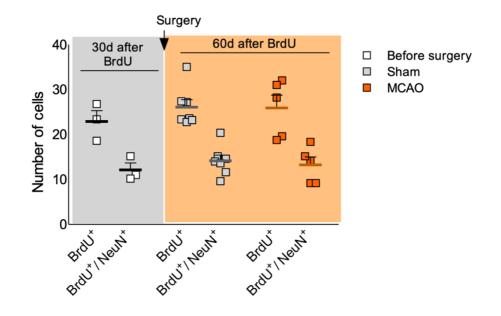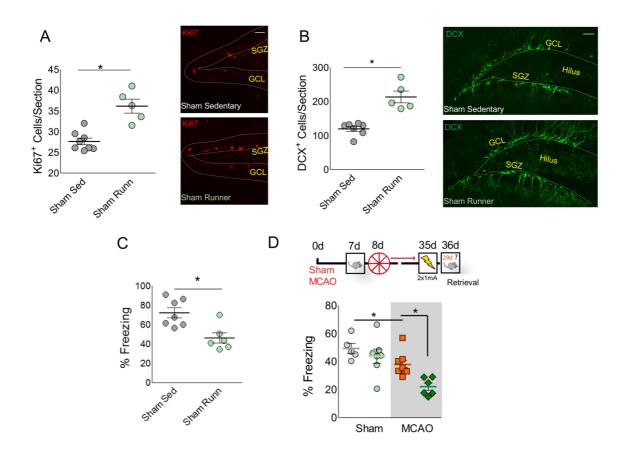
Supplementary figure 6. Post-stroke neurogenic response does not correlate with lesion size. (A-B) Spearman correlation analysis of hippocampal DCX$^+$ cells in ischemic mice with the percentage of infarcted hemisphere determined by MRI 48h after stroke onset (A, n=31, Spearman r=0.05848, p>0.05) or with the final lesion size at 35 days displayed as % lost ipsilateral cortex (B, n=21, Spearman r=0.03899, p>0.05). Data are mean ± SEM. Data were compared by using nonparametric 2-tailed Spearman correlation.
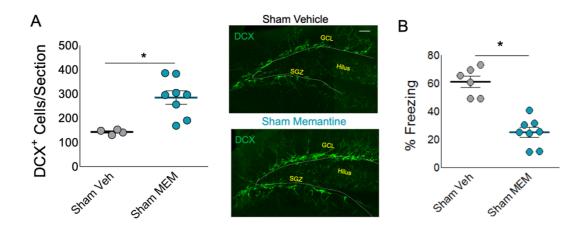
Supplementary figure 7. Cortical ischemia does not affect postnatal generated neurons. Quantification of BrdU$^+$ neurons generated during postnatal development (p30). BrdU was administered at p30 and colocalization analysis with neuronal marker calbindin was performed just before ischemia (30 days after BrdU administration) and 1 month after surgery (60 days after BrdU administration). (Before surgery, n=3; sham, n=7; MCAO, n=5). Data are mean ± SEM. Data were compared by using nonparametric 2-tailed Mann-Whitney tests.
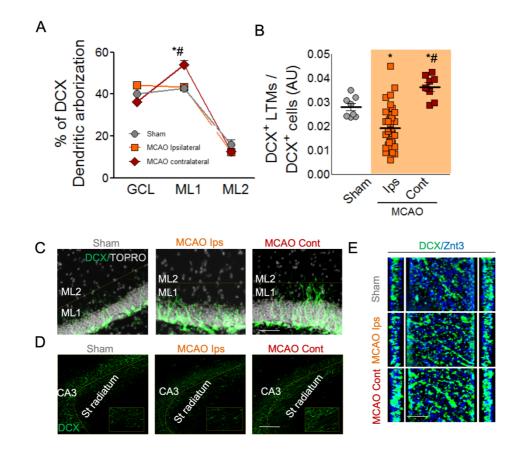
Supplementary figure 8. Increasing hippocampal neurogenesis by running impairs recall in mice. **(A-B)** Number of Ki67^{+} (A) and DCX[+] (B) cells in sedentary and running sham mice (*p<0.05 vs. sham sed; sham sed=7-8, sham runner=5). Representative images are displayed on the right. Scale bar: 30 μm. **(C)** Percentage of freezing response in sedentary and runner sham mice 28 days after contextual fear conditioning (CFC; *p<0.05 vs. sham veh; sham sed=7, sham runner=6). **(D)** In top**,** experimental design for incidental context learning. Seven day after ischemia, mice were exposed to conditioning chamber for 10 minutes but not foot-shock were presented. 28 days later, mice were re-exposed to conditioning chamber and received 2 foot-shocks. Mice were tested 24h later. In the bottom graph**,** the percentage of freezing response in sedentary and runner sham and MCAO mice in the incidental context paradigm. Two-way ANOVA demonstrated a significant effect of both MCAO (F(1,22)= 18.05; p=0.0003) and running ((F(1,22)= 7.54; p=0.0118); Bonferroni post-hoc: *p<0.05; sham sedentary, n=5; sham runner, n=7; MCAO sedentary, n=8; MCAO runner, n=6). Data are mean ± SEM. Data were compared by using nonparametric 2-tailed Mann-Whitney tests or a nonparametric 2-way ANOVA followed by Bonferroni post hoc testing.
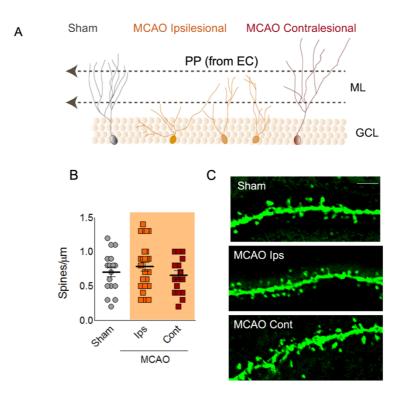
Supplementary figure 9. Increasing hippocampal neurogenesis by memantine impairs recall in mice. **(A)** Quantification of neuroblasts in vehicle and memantine (MEM)-treated sham mice (*p<0.05 vs. sham MEM; sham veh, n=4; sham MEM, n=8). Representative images are displayed on the right. Scale bar: 30 µm. **(B)** Percentage of freezing response after MEM treatment 28 days after CFC (*p<0.05 vs. sham veh; sham veh, n=6; sham MEM, n=8). Data are mean ± SEM. Data were compared by using nonparametric 2-tailed Mann-Whitney tests.

Supplementary figure 10. Altered features of immature DCX$^+$ neurons induced by stroke. (A) Analysis of the % of DCX$^+$ dendritic arborisation distributed along granule cell layer (GCL) and molecular layer (ML) in sham and ischemic mice 35 days after ischemia. Two-way ANOVA demonstrated a significant interaction between DCX$^+$ distribution and experimental group ($F_{(1,16)}$= 4.84; p=0.0040) (Bonferroni post-hoc; *#p<0.05 vs. sham and MCAO ipsilesional, respectively; sham, n=7; MCAO ipsilesional, n=12; MCAO contralesional, n=12). **(B)** DCX$^+$ long mossy fibre terminals (LMTs) found in the *stratum lucidum* of CA3 in sham and ipsi- and contralesional sides of ischemic mice. Data are displayed as the ratio between DCX-LMTs in CA3 and DCX$^+$ cells in DG (*#p<0.05 vs. sham and MCAO ipsilesional, respectively; sham, n=7; MCAO ipsilesional, n=12; MCAO contralesional, n=12). (**C-D**) Representative images of GCL/ML DCX$^+$ dendritic arborisation (C, scale bar: 75µm) and DCX$^+$ staining in CA3 (green) (D, scale bar: 100µm). TOPRO was used as nuclear marker. **(E)** Reconstructions of DCX (green) staining in combination with the post-synaptic marker Znt3 (blue) in the CA3 *stratum lucidum* of sham and ischemic mice showing DCX$^+$ LMTs in closed apposition with Znt3; scale bar: 10µm. Data are mean ± SEM. Data were compared by using nonparametric 2-tailed Mann-Whitney tests or a nonparametric 2-way ANOVA followed by Bonferroni post hoc testing.
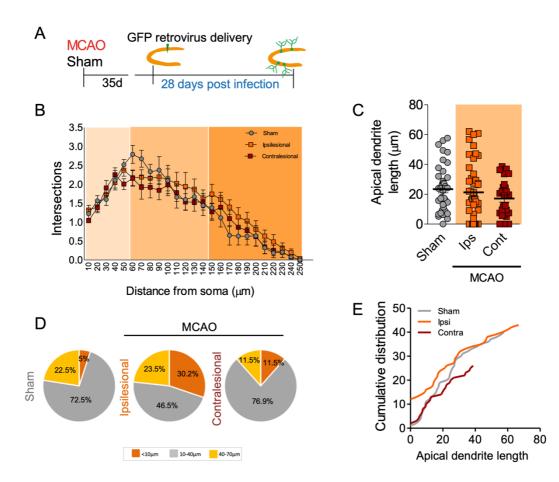
Supplementary figure 11. Aberrant features of GFP newborn neurons after stroke.
(A) Reconstructions of GFP retroviral labelled neurons observed in each experimental group and their location in the GCL; PP (perforant pathway); EC (entorhinal cortex). **(B)** Spine density analysis of mature newborn granule neurons of DG in sham and ischemic mice 28 days post infection (dpi) with a GFP retrovirus (p>0.05; sham, n=18neurons/3 mice; MCAO Ips, n=23neurons/4mice; MCAO Cont, n=17neurons/3mice). **(C)** Representative images of spine density in the outer molecular layer segment of newborn granule neurons in sham and ischemic mice 28 dpi. Scale bar: 5µm. Data are mean ± SEM. Data were compared by using nonparametric 2-tailed Mann-Whitney tests.
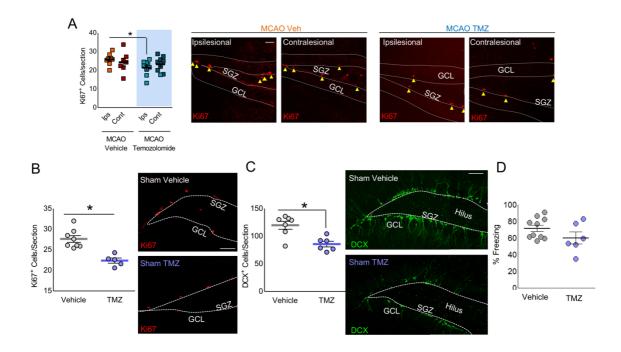
Supplementary figure 12. Aberrant features of new generated neurons after stroke.
(A) Experimental design for retrovirus infusion after ischemia used in panels B-D. **(B)** Sholl analysis of GFP-retrovirally infected newborn neurons in the dentate gyrus of sham and MCAO, 28 days after infection. No differences were observed in the number of intersections in the different experimental groups by two-way ANOVA analysis ($p > 0.05$; sham: n=42neurons/7mice; MCAO ipsilesional: n=44neurons/8mice; MCAO contralesional: n=32neurons/8mice). **(C)** Quantification of apical dendritic length (sham: n=42neurons/7 mice; MCAO ipsilesional: n=44 neurons/8 mice; MCAO contralesional: n=32neurons/8mice). **(D)** Pie charts display the percentage of GFP$^+$ neurons in each experimental group showing apical dendrite lengths of <10µm, 10-40µm and >40µm (sham, n=42neurons/7mice; MCAO ipsilesional, n=44neurons/8mice; MCAO contralesional, n=32neurons/8mice). **(E)** Cumulative distribution of apical dendrite length in different experimental conditions ($p < 0.05$, MCAO ipsilesional vs. sham; sham: n=42 neurons/7mice; MCAO ipsilesional: n=44neurons/8mice; MCAO contralesional: n=32neurons/8mice. Data are mean ± SEM. Data were compared by using nonparametric 2-tailed Mann-Whitney tests or a nonparametric 2-way ANOVA followed by Bonferroni post hoc testing.

Supplementary figure 13. Effect of hippocampal neurogenesis inhibition by temozolomide. (A) Quantification of Ki67$^+$ cells in MCAO mice treated with vehicle or temozolomide (TMZ). Representative images of Ki67$^+$ (red) in MCAO mice treated with vehicle or TMZ are shown in the right panel. Scale bar: 30µm. Two-way ANOVA analysis showed a significant effect of TMZ in the number of Ki67$^+$ cells at 35 days (F(1,30)= 5.09; p=0.0315) (Bonferroni post-hoc: *p<0.05 vs. MCAO vehicle; MCAO vehicle, n=8; MCAO TMZ, n=9). **(B-C)** Number of Ki67$^+$ (B) and DCX$^+$ (C) cells in sham mice treated either with vehicle or temozolomide (TMZ), analyzed 35 days after surgery (*p<0.05 vs. vehicle; sham veh, n=7; sham TMZ, n=5). Representative images of Ki67$^+$ cells (red) and DCX$^+$ cells (green) are shown in the right panels. Scale bar: 30µm. **(D)** Percentage of freezing response in vehicle- and temozolomide-treated mice 35d after surgery (p>0.05; sham vehicle, n=10; sham TMZ, n=6). Data are mean ± SEM. Data were compared by using nonparametric 2-tailed Mann-Whitney tests or a nonparametric 2-way ANOVA followed by Bonferroni post hoc testing.

Supplementary figure 14. Effect of conditional deletion of hippocampal neurogenesis. (A) Quantification of DCX$^+$ cells in sham vehicle and tamoxifen-treated Nestin-Cre^{ERT2}/NSE-DTA (*p<0.05 vs. vehicle-treated Nestin-Cre^{ERT2}/NSE-DTA sham mice; sham vehicle=7; sham tamoxifen=5). **(B)** Representative images of DCX$^+$ cells in Nestin-Cre^{ERT2}/NSE-DTA sham mice treated with vehicle (left) or tamoxifen (TAM) (right). Scale bar: 30µm. **(C)** Percentage of freezing response in vehicle and tamoxifen-treated Nestin-Cre^{ERT2}, and in vehicle and tamoxifen-treated Nestin-Cre^{ERT2}/NSE-DTA mice 28 days after contextual fear conditioning (*p<0.05 vs. vehicle-treated Nestin-Cre^{ERT2}; #p<0.05 vs. vehicle-treated Nestin-Cre^{ERT2}/NSE-DTA; Nestin-Cre^{ERT2} vehicle, n=9; Nestin-Cre^{ERT2} tamoxifen, n=8; Nestin-Cre^{ERT2}/NSE-DTA vehicle, n=16; Nestin-Cre^{ERT2}/NSE-DTA tamoxifen, n=20). Data are mean ± SEM. Data were compared by using nonparametric 2-tailed Mann-Whitney tests or a nonparametric 2-way ANOVA followed by Bonferroni post hoc testing.